





Surface functionalization of microporous carbon fibers by vapor phase methods for CO₂ capture

Special Collection: [Atomic Layer Deposition \(ALD\)](#)

Stephan Prünke ; Gerben van Straaten; Dries van Eyck; Oscar Diaz-Morales ; Jeroen Van Dijk ; Hans de Neve; Mariadriana Creatore 



J. Vac. Sci. Technol. A 41, 032403 (2023)

<https://doi.org/10.1116/6.0002419>



View
Online



Export
Citation

CrossMark

Related Content

Quartz crystal microbalance study of precursor diffusion during molecular layer deposition using cyclic azasilane, maleic anhydride, and water

Journal of Vacuum Science & Technology A (April 2019)

Molecular layer deposition using cyclic azasilanes, maleic anhydride, trimethylaluminum, and water

Journal of Vacuum Science & Technology A (December 2016)



Instruments for Advanced Science

- Knowledge
- Experience
- Expertise

Click to view our product catalogue

Contact Hiden Analytical for further details:
www.HidenAnalytical.com
info@hiden.co.uk

Gas Analysis



- dynamic measurement of reaction gas streams
- catalysis and thermal analysis
- molecular beam studies
- dissolved species probes
- fermentation, environmental and ecological studies

Surface Science



- UHV/TPD
- SIMS
- end point detection in ion beam etch
- elemental imaging - surface mapping

Plasma Diagnostics



- plasma source characterization
- etch and deposition process reaction kinetic studies
- analysis of neutral and radical species

Vacuum Analysis



- partial pressure measurement and control of process gases
- reactive sputter process control
- vacuum diagnostics
- vacuum coating process monitoring

Surface functionalization of microporous carbon fibers by vapor phase methods for CO₂ capture

Cite as: J. Vac. Sci. Technol. A 41, 032403 (2023); doi: 10.1116/6.0002419

Submitted: 13 December 2022 · Accepted: 10 February 2023 ·

Published Online: 15 March 2023



Stephan Prünte,^{1,a)} Gerben van Straaten,^{2,3} Dries van Eyck,³ Oscar Diaz-Morales,³ Jeroen Van Dijk,³ Hans de Neve,³ and Mariadriana Creatore^{2,4}

AFFILIATIONS

¹Institute of Energy and Climate Research, Materials Synthesis and Processing (IEK-1), Forschungszentrum Jülich GmbH, 52428 Jülich, Germany

²Department of Applied Physics and Science Education, Eindhoven University of Technology, 5600 MB Eindhoven, The Netherlands

³Carbyon, High Tech Campus 27, 5656 AE Eindhoven, The Netherlands

⁴Eindhoven Institute of Renewable Energy Systems (EIRES), 5600 MB Eindhoven, The Netherlands

Note: This paper is part of the 2023 Special Topic Collection on Atomic Layer Deposition (ALD).

a) Author to whom correspondence should be addressed: s.prunte@fz-juelich.de

ABSTRACT

The removal of excess CO₂ from the atmosphere is expected to play a major role in the mitigation of global warming. Solid-state adsorbents, consisting of CO₂-binding functionalities on porous supports, can provide high CO₂ capture capacities with low energy requirements. In this contribution, we report on the vapor-phase functionalization of porous carbon fibers with amine functionalities. Functionalization occurs either via direct exposure to cyclic azasilane molecules (2,2-dimethoxy-1,6-diaza-2-silacyclooctane) or by the atomic layer deposition of Al₂O₃ followed by exposure to azasilane. XPS analysis and SEM/energy-dispersive x-ray spectroscopy (EDX) measurements confirmed Al₂O₃ deposition and amine functionalization. Yet, the two different functionalization approaches led to different amine loadings and distinct differences in porosity upon functionalization, which affected CO₂ capture. Combining Al₂O₃ and amine functionalization resulted in fast CO₂ sorption with superior capturing efficiency. In contrast, direct functionalization resulted in strong reduction of the surface area of the porous support and limited gas exchange. We attribute the superior capture efficiency to the porosity level achieved when combining Al₂O₃ and amine functionalization demonstrating that this approach might be valuable for compact high-throughput direct air, CO₂ capture systems.

© 2023 Author(s). All article content, except where otherwise noted, is licensed under a Creative Commons Attribution (CC BY) license (<http://creativecommons.org/licenses/by/4.0/>). <https://doi.org/10.1116/6.0002419>

I. INTRODUCTION

Mitigation of global warming in accordance with the Paris climate agreement demands suppressing CO₂ emission. Besides these ambitious efforts, the removal of excess CO₂ from the atmosphere by sequestration technologies is equally relevant to meet international climate goals.^{1–4} Climate modeling where global warming is limited to 1.5 °C by 2100 indicates that CO₂ removal in the range of 20–660 × 10⁹ t is a mandatory step.⁵ Apart from technologies that immediately sequester CO₂ from the exhaust of fossil fuel power plants, direct air capture (DAC)^{6,7} removes CO₂ from the ambient air by employing either liquid solvents⁸ or solid

sorbents.⁹ DAC is essential for industries that cannot easily be decarbonized, e.g., aviation, construction, and heavy transportation, to meet their contribution in the reduction of CO₂ emission. Moreover, the regeneration of either solvent or sorbent generates CO₂-rich streams that can be utilized for the production of chemicals or synthetic fuels, or alternatively, to improve crop yield in greenhouses.¹⁰ In conclusion, efficient and scalable DAC technologies are required.

Alkaline solvents and solid sorbents employing amine functionalities on porous supports are the most mature DAC approaches⁶ and have been already commercialized, e.g., by

22 September 2023 08:53:50

Climeworks^{11,12} and Carbon Engineering.⁸ While DAC by liquid solvents requires high temperatures of up to 900 °C to regenerate the solvent,⁸ the release of CO₂ from amine functionalities on solid sorbents occurs at lower temperatures, i.e., between 80 and 120 °C,^{7,13–15} allowing for smaller feasible scales of DAC plants using amine-based solid sorbents.⁶ As a result, life cycle assessments of DAC plants employing liquid absorption revealed CO₂ emission of 400–510 g CO₂ per captured kg of CO₂ due to heat generation by fossil fuel.^{16,17} For DAC by amine-based solid sorbents, the choice of the support is crucial as it strongly affects the overall carbon footprint with CO₂ emission of 15 g per captured kg of CO₂ for sorbents made from amines on Al₂O₃ compared to 45 g of CO₂ emitted per captured kg of CO₂ for amines on cellulose supports.¹² Hence, further research is necessary to explore other sorbent-support combinations for DAC.

Several studies^{15,18–20} revealed the importance of the porous nature of the support on CO₂ capture capacity, preferably combining a high degree of porosity with a large internal surface.¹⁵ While commonly used mesoporous supports (pore diameter 2–50 nm) are characterized by surface areas of <1000 m² for the blank support, amine functionalization further reduces this figure (Table I). It was observed that under specific conditions, pore filling detrimentally affected CO₂ capture capacities,²⁴ as it reduced adsorption sites available for CO₂. To increase the adsorption sites and, hence, CO₂ capture capacities, the present work explores the capabilities of amine-functionalized activated carbon fibers (ACFs) as solid sorbents for direct air capture. ACFs are characterized by large surface areas (up to 2000 m²/g) up to 87% porosity and pore diameter <2 nm.³⁰ While ACF have also been studied to capture CO₂ from flue gas either by pristine fibers³¹ or by alkaline carbonate immersion,^{32–34} we aim to functionalize the internal surface of ACFs with single layers of chemisorbed amines to capture CO₂ directly from ambient air. In the present study, microporous ACF was chosen as the support revealing distinct pore diameter ranges of 0.3, 0.5–0.6, and 0.8 nm. It must be added that a metal-organic framework (MOF) may constitute as an alternative to ACF adsorbents. However, the high costs of MOF adsorbents compared to those based on ACF leave this alternative as economically not

feasible.³⁵ Recently, polymer fiber materials are also explored for DAC applications but functionalized with polyamines.^{29,36}

Besides porosity, the thermal properties of the porous support are also relevant, as the sorbent is heated to temperatures of 80–120 °C to release the captured CO₂. The thermal conductivity of ACF was reported to be one order of magnitude higher³⁷ compared to mesoporous silica.^{38,39} Moreover, ACFs are electrically conductive allowing for resistive heating and, hence, help to operate ACF-based DAC facilities on electricity from renewable resources and simplify their design and daily operation.

Prior to the regeneration of the sorbent, CO₂ capture occurs by chemical reactions between primary (R-NH₂) or secondary (R₁R₂-NH) amines and CO₂ resulting in the formation of carbamates, carbamic acid, and bicarbonates, as explained and illustrated in the supplementary material.⁷³ These reactions occur with high selectivity even at very low CO₂ partial pressure as in ambient conditions (ca. 400 ppm).⁷ While the formation of carbamic acid and ammonium carbamates has been observed under dry^{40,41} and humid^{41–43} conditions, the CO₂-binding reaction via the bicarbonate path requires a humid atmosphere,^{40,44} which is usually the case for DAC. More importantly, the amine efficiency, i.e., the amount of CO₂ captured per mole of amine functionalities, can be up to 1 for carbamic acid and bicarbonate path compared to 0.5 when carbamates are formed since two amine functionalities are necessary to react with one CO₂ molecule to form ammonium carbamate [Eqs. (1)–(3) and Fig. S1 in the supplementary material].^{7,73} Recent *in situ* experiments revealed the intramolecular formation of carbamates by the primary and secondary amine functionalities present in a diamine,⁴⁰ implying that steric limitations in CO₂ capturing by the carbamate path might be overcome when employing diamines as CO₂ capturing functionalities.

Besides high CO₂ selectivity in DAC-relevant conditions, the designated amine should chemisorb on the internal surface of the microporous ACF (pore diameter < 1 nm) to avoid stability issues commonly occurring for sorbents made by amine impregnation.⁴⁵ Moreover, impregnation or polymerization with polyamine will cause the clogging of microporosity and, hence, negatively affects gas exchange during DAC. Linear di- or tri-amines used to prepare

TABLE I. Examples of porous supports and amine-functionalized sorbents fabricated by different techniques for CO₂ capture at DAC-relevant conditions.

| Support | Surface area (m ² /g) | | Functionalization technique | Reference |
|---|----------------------------------|------------------------------|-----------------------------|-----------|
| | Blank support | Amine-functionalized sorbent | | |
| Mesoporous SiO ₂ foam | 563–648 | 230–344 | Grafting | 15 |
| SiO ₂ gel beads | 422 | 216 | Grafting | 13 |
| Pore-expanded SiO ₂ | 950 | 367 | Grafting | 21,22 |
| Mesoporous SiO ₂ | 880 | 240–470 | Impregnation | 23 |
| Mesoporous SiO ₂ | 700 | 400–30 | Impregnation | 24 |
| Mesoporous SiO ₂ | 840 | 579–45 | Polymerization | 25 |
| Mesoporous Al ₂ O ₃ | 234 | 29–111 | Impregnation | 26 |
| Graphene oxide | 289 | 198 | Grafting | 27 |
| MOFs | 1094 | 469 | Grafting | 28 |
| Polymer/SiO ₂ fibers | 106 | 11 | Impregnation | 29 |
| ACF cloth | 1460 | 760–1050 | Grafting | This work |

DAC sorbents by grafting^{13,21,22,27} (Table S1 in the supplementary material)⁷³ are usually ≥ 1 nm in length, which will not only detrimentally affect gas exchange in microporous ACF during DAC, but also the diffusion-based penetration of these molecules while manufacturing the sorbent. To overcome this problem, diamine functionality is provided in this work by a cyclic azasilane (2,2-dimethoxy-1,6-diaza-2-silacyclooctane) molecule with a diameter of approximately 0.6 nm guaranteeing penetration in ACF microporosity. Here, chemisorption occurs by the ring-opening reaction with hydroxyl groups present at the surface of the substrate.^{46–48} The Si-N bond in cyclic azasilane is cleaved due to the higher stability of the Si-O bridge compared to Si-N.^{49,50} Two different strategies are investigated to functionalize the porous ACF substrate either by direct exposure of azasilane or by the atomic layer deposition (ALD) of Al_2O_3 prior to amine functionalization with azasilane. Both approaches are evaluated based on chemistry, homogeneity, porosity, and CO_2 capture under conditions close to industrial DAC. Herein, we observed that both amine functionalization strategies resulted in CO_2 capture. Yet, the approach involving the ALD of Al_2O_3 prior to amine functionalization caused superior efficiency in CO_2 capturing, compared to direct amine functionalization of the ACF cloth. Different CO_2 capturing behavior can be rationalized by the difference in the internal surface and pore-size distribution resulting from the two functionalization approaches.

II. EXPERIMENT

Sheets of the ACF cloth (FM50K, Chemviron Carbon Ltd., UK) were cut in squares of $60 \times 60 \text{ mm}^2$, dried at 140°C in a glove-box containing N_2 (H_2O , $\text{O}_2 < 0.1 \text{ ppm}$), stored in sealed vials, and weighed on a microgram scale (Mettler, Switzerland). Vapor-phase-based surface functionalization of the ACF sheets was carried out in a vacuum ALD reactor (base pressure = $1 \times 10^{-4} \text{ Pa}$, described in Ref. 51). The substrate table and reactor walls were heated to 125°C . Vapors of azasilane (Fluorochem, UK) were supplied to the reactor in multiple dosing pulses of 2 s from a stainless steel bubbler heated to 90°C using Ar as the carrier gas, while the reactor chamber was isolated from the pumps for 10 s to allow for precursor diffusion into the porous ACF. Subsequently, the reactor was evacuated for 10 s resulting in base pressures below $1 \times 10^{-2} \text{ Pa}$. ALD Al_2O_3 modification of the ACF cloth prior to amine functionalization was performed using the same experimental setup and conditions used for azasilane modification, namely, the same wall and substrate table temperatures. Multiple pulses of trimethylaluminum (TMA, Sigma-Aldrich Chemie BV, The Netherlands) heated to 30°C and dosed for 100 ms per pulse were introduced into the reactor chamber which was isolated from the pumps for 30 s during each pulse. After TMA dosing, an equal pulse number of 100 ms H_2O vapor was introduced into the evacuated reactor from a steel flask containing H_2O (technical grade, VWR International S.A.S., France) kept at room temperature. Amino-functionalized and ALD Al_2O_3 -modified sheets of the ACF cloth were again dried, stored in vials, and weighed as described above to measure the weight gain caused by functionalization. Amine loadings in $\text{mmol}_\text{N}/\text{g}_\text{sorbent}$ were derived from the measured weight gain.

X-ray photoelectron spectroscopy (XPS) measurements were performed on small coupons cut from the functionalized sheets in a K-Alpha instrument (Thermo Fisher Scientific, UK) using monochromated $\text{Al}_{K\alpha}$ radiation with a $400 \mu\text{m}$ spot-size and a charge-neutralizing flood-gun. The Advantage software package (Thermo Fisher Scientific, UK) was employed for measurement and analysis using standard conditions of the instrument for survey and high-resolution scans as well as charge correction with the C 1s signal at 284.8 eV.

The cross section of functionalized ACF prepared by cutting with a scalpel blade was investigated in a NovaNanoLab600i (FEI Company, USA) scanning electron microscope (SEM) equipped with a Genesis XM 4i Si(Li) detector (EDAX Inc., USA). Energy-dispersive x-ray spectroscopy (EDX) was employed to map the chemical composition of the fiber cross section measuring >100 frames of 128×128 pixel with 5 kV accelerating voltage for the electron beam.

The surface area was measured by Brunauer-Emmett-Teller (BET) analysis. Ar isotherms were measured at 87 K on an Autosorb AS1 (Quantachrome Instruments, USA). The samples (both pristine and functionalized) were first degassed at 60°C for 16 h to remove all adsorbed species from the surface. Pore-size distributions were derived from CO_2 adsorption isotherms at 273 K on an Autosorb ASiQ (Quantachrome Instruments, USA) after degassing the samples at 60°C for 16 h. Calculations of pore-size distribution were performed using the nonlocal density functional theory method⁵² (CO_2 adsorbate at 273 K with a carbon adsorbent) embedded in the ASiQ measurement software.

CO_2 sorption measurements were conducted in a hermetically sealed gas exposure setup coupled with a mass-spectrometer. Samples of functionalized and pristine ACF cloth were exposed to synthetic air containing 400 ppm CO_2 for 3600 s at a flow rate of 1 l/min. For humid adsorption conditions, synthetic air was led through a controlled evaporation unit (Bronkhorst High-Tech B.V., the Netherlands) and exposed to H_2O prior to sample exposition. Subsequently, the samples were heated to 80°C for CO_2 desorption and purged by N_2 stream (0.1 l/min for 3000 s) fed via a heated quartz inlet capillary to a quadrupole mass-spectrometer (HPR-20 R&D, Hiden Analytical, UK) to determine the amount of desorbed CO_2 captured by the samples during exposure to synthetic air. All samples were purged at RT for 20 min with N_2 at a 1 l/min flow rate between CO_2 adsorption and desorption without exposure to ambient air. All gases used for processing and analysis were of 99.999% purity.

III. RESULTS AND DISCUSSION

A. Characterization of functionalized ACF cloth samples

After vapor-phase-based surface functionalization and sample drying, modified sheets of ACF reveal a weight gain compared to the initial sample weight (Fig. 1). The weight gain saturated (i.e., plateau reached in the plots of Fig. 1), for which the saturation condition depended on the functionalization route. Saturation of the weight gain occurs after 50 dosing pulses at 11% for ALD Al_2O_3 [Fig. 1(a)] and after 800 and 200 dosing pulses of amine functionalization [Fig. 1(b)] on pristine and ALD Al_2O_3 -modified ACF

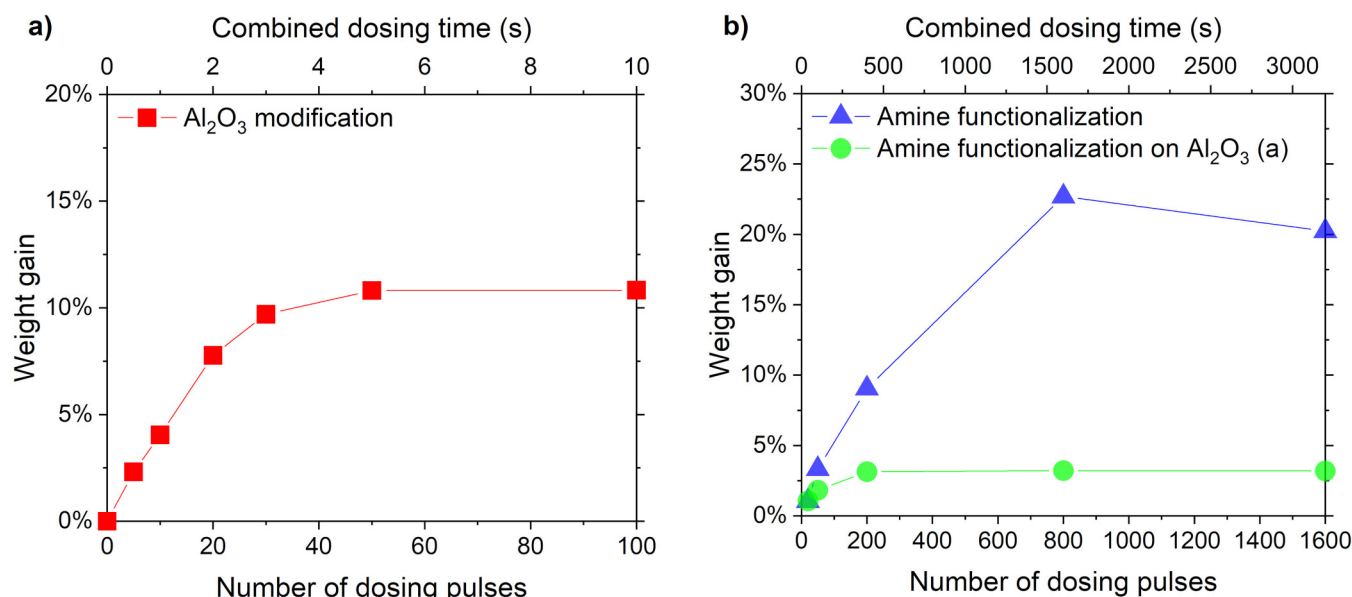


FIG. 1. Saturation curves of (a) Al_2O_3 -modified ACF cloth and of (b) amine functionalization introduced directly to ACF cloth or after Al_2O_3 modification. Measured values are subjected to an experimental error of $\pm 0.6\%$.

cloth samples, respectively. A maximum weight gain of 3% was observed for amine functionalization on ALD Al_2O_3 -modified ACF cloth samples. This figure changed to 20%–23% for direct amine functionalization on pristine ACF. To estimate the experimental error, 15 ACF cloths were modified with 100 dosing pulses of ALD Al_2O_3 , which resulted in a sample standard deviation of $\pm 0.6\%$ in weight gain.

The decrease in weight gain observed for amine functionalization on pristine ACF with 1600 dosing pulses might be explained by small differences in the porosity of the ACF samples observed for commercial ACF.⁵³ Independently from the selected route, the different functionalization routes result in saturation, as it is depicted in the weight gain plot of Fig. 1. Results presented in Table II, Fig. 2, and Sec. III B refer to the saturation condition.

XPS was performed on all functionalized and pristine ACF samples. Chemical composition (Table II) reveals large relative concentrations of Si and N for the amine-functionalized surfaces compared to the pristine ACF cloth, which may contain residual N, as polyacrylonitrile (PAN) fibers are used as initial fibers in the production of ACF utilized in this work. Additionally, pristine ACF

contained Al, Zn, and minor traces of Ca and Cl. All these elements are used either in the stabilization of raw PAN fibers or in the chemical activation process for manufacturing PAN-based ACF.^{53,54}

Detailed spectra are recorded for the elements present in the Al_2O_3 and amine-functionalized samples (Fig. 2). Chemical states indicated in Fig. 2 are attributed to the binding energies of peaks obtained by the deconvolution and peak fitting of all detailed spectra. Fitting parameters are given for all detailed spectra (Tables S2–S5 in the supplementary material)⁷³ and the deconvolution of all C 1s spectra (Fig. S3 in the supplementary material).⁷³ The N 1s spectrum is detected for amine-functionalized surfaces with a major contribution at a binding energy of 399.6 eV [Fig. 2(a)], associated to nonprotonated amines.^{55–57} Deconvolution (Table S2 in the supplementary material)⁷³ revealed similar amounts (18% peak area) of protonated amines (401.7–402.0 eV)^{55–57} for both functionalized surfaces. This indicates that the exposure of pristine and Al_2O_3 -modified ACF to azasilane results in an amine-functionalized surface, which should be prone to capture CO_2 . Pristine and Al_2O_3 -modified ACF cloth samples revealed a minor

TABLE II. Chemical composition of pristine and functionalized ACF derived by XPS.

| Sample | C (at. %) | O (at. %) | Al (at. %) | N (at. %) | Si (at. %) | Zn (at. %) | Ca (at. %) | Cl (at. %) |
|---------------------------------|-----------|-----------|------------|-----------|------------|------------|------------|------------|
| Pristine | 61.0 | 24.1 | 9.8 | 1.7 | 0.1 | 3.1 | 0.3 | 0.1 |
| Al_2O_3 | 36.9 | 42.2 | 12.9 | 1.3 | 0.0 | 5.1 | 0.0 | 1.6 |
| Al_2O_3 + Amine | 53.7 | 27.5 | 10.4 | 5.1 | 1.9 | 1.1 | 0.2 | 0.1 |
| Amine | 59.8 | 22.1 | 7.7 | 5.9 | 2.4 | 1.9 | 0.2 | 0.1 |

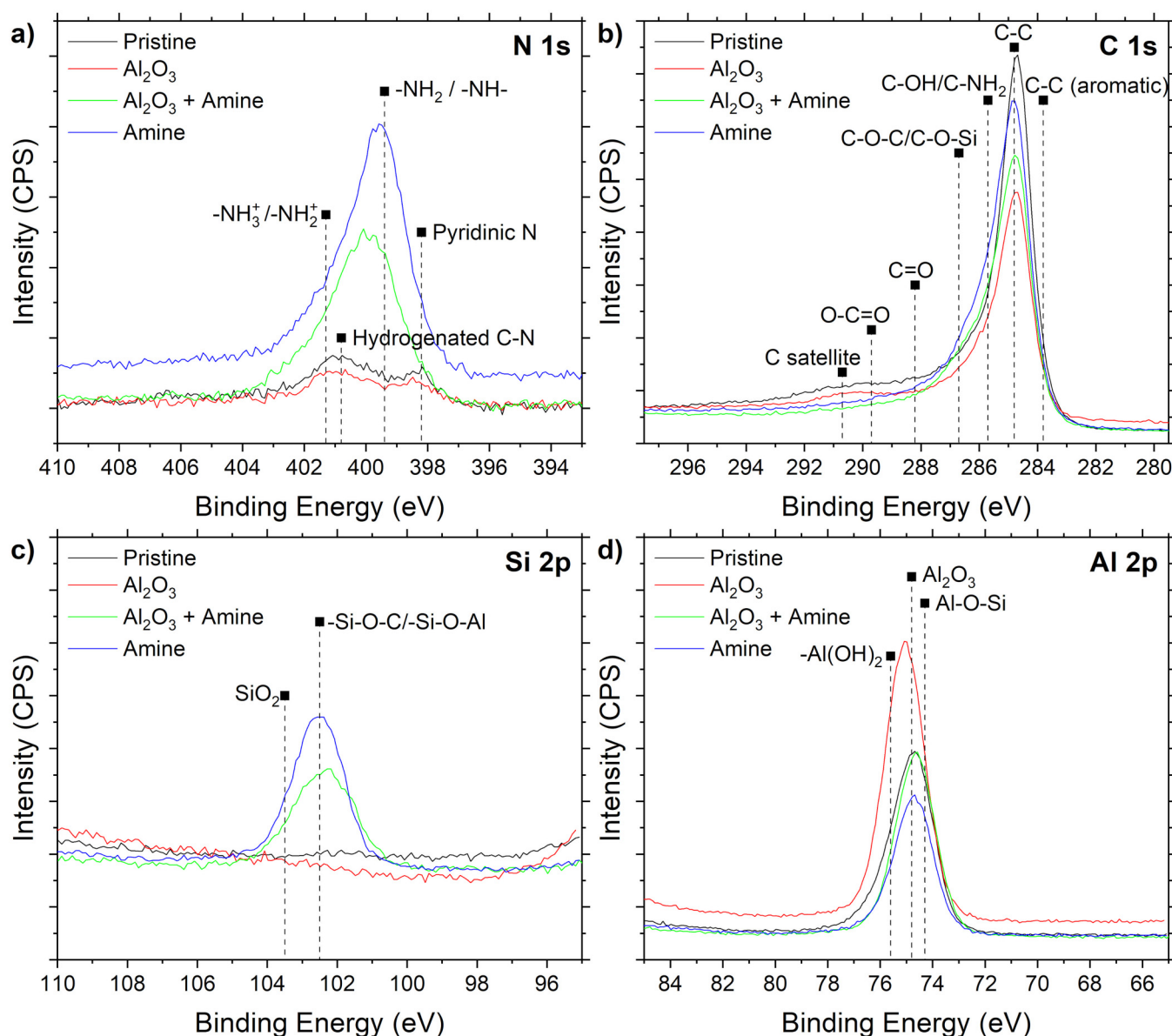


FIG. 2. Spectra of pristine and functionalized ACF obtained by XPS: N 1s (a), C 1s (b), Si 2p (c), and Al 2p (d).

contribution of the N 1s signal most certainly originating from hydrogenated C–N bonds^{56,58} and pyridinic N (Refs. 56 and 59) from the PAN fibers used for ACF fabrication.⁵³

The C 1s spectrum from all samples reveals a large contribution of graphitic/aliphatic carbon at 284.8 eV [Fig. 2(b)]. A shoulder at 286.5 eV was observed for the amine-functionalized sample suggesting a higher contribution of C–O–Si bridges,⁶⁰ notwithstanding the partial overlap with C–OH and C–O–C bonds at 285.7 and 287.1 eV,^{61,62} respectively. Compared to the pristine sample,

this contribution increases twofold (Table S3 in the supplementary material)⁷³ for amine and Al₂O₃ plus amine-functionalized surface, respectively. This observation gives a first indication of the chemical anchoring of ACF exposed to azasilane vapor, further disclosed in the Si 2p spectra.

Si [Fig. 2(c)] is only detected for amine-functionalized ACF. Both amine and Al₂O₃- and amine-functionalized samples revealed the presence of Si 2p signals at 102.4–102.5 eV associated to (–SiO₃) anchoring the azasilane molecule by Si–O–C bridges to the

surface of ACF.^{60,63} The signal below binding energies of 98 eV observed for Al₂O₃-modified ACF belongs to the Zn 3p spectrum (peak binding energy of ~89–91 eV)⁶⁴ caused by a large amount of Zn (5.1 at. %, Table II) detected in the Al₂O₃-modified sample. As both functionalization approaches promoted the formation of Si-O-C anchoring on pristine and Al₂O₃-modified ACF, the ring-opening anchoring reaction of cyclic azasilane occurred on these surfaces. While hydroxyl groups facilitate reactive sites for the ALD Al₂O₃-modified ACF,⁶⁵ pristine ACF revealed epoxy, carbonyl, and carboxyl groups in the C 1s signal (Table S3 in the supplementary material).⁷³ Although hydroxyl and epoxy groups overlap with C-NH₂ and C-O-Si bonds, respectively, the amount of carboxyl groups is reduced as well for amine-functionalized ACF [Fig. 2(b)] by 30% indicating that the azasilane molecules also reacted with the carboxyl groups in the pristine ACF surface (Table S3 in the supplementary material).⁷³

Aluminum [Fig. 2(d)] is detected in all samples due to the aforementioned process-induced Al₂O₃ (Ref. 53) observed on the outside of the fibers (Fig. S6 in the supplementary material).⁷³ Peak binding energies were observed from 74.7 to 75.0 eV attributed to Al₂O₃.^{66,67} Yet, the Al 2p signal originating from ALD Al₂O₃ modification revealed a higher intensity compared to Al 2p signals from the other samples. Hence, Al₂O₃ modification by one ALD cycle introduced -Al(OH)₂ terminations to the internal surface of ACF due to the termination of the ALD cycle with H₂O doses. However, the symmetric Al 2p signal [Fig. 2(d)] observed for all samples renders the distinction between -Al(OH)₂ terminations (binding energy at 75.6 eV)⁶⁸ and Al₂O₃ and the determination of the amount of -Al(OH)₂ terminations as impossible. Al-OH termination also provides reactive sites toward azasilane for amine functionalization. The resultant Si-O-Al bridges are expected at binding energies of 74.3 eV.⁶⁹ However, it cannot be discriminated between -Si-O-C and -Si-O-Al bridges for the Al₂O₃ plus amine-functionalized sample again due to the symmetric signal obtained in the Al 2p spectra.

Since XPS probes only the first few nanometers of the surface, EDX-mapping is adopted to investigate the distribution of Al₂O₃ and amine functionalization over fiber cross sections (Fig. 3). Cross sections of the Al₂O₃ and Al₂O₃ plus amine-functionalized samples reveal Al present and homogeneously distributed in the center of the fiber [Figs. 3(b) and 3(c)]. While Al is mostly observed on the edge of pristine ACF [Fig. 3(a)] and, to smaller extents, on the directly amine-functionalized fiber [Fig. 3(d)], the center of these fibers contains little Al compared to Al₂O₃-modified ACF [Figs. 3(b) and 3(c)]. Most likely, the observed Al agglomerations on the edge of the cross sections originate from the industrial preparation process of pristine ACF, as analyzed by SEM and EDX in Fig. S6 in the supplementary material,⁷³ caused by the chemicals used during the processing and activation of ACF.⁵³ Chemical compositions measured by EDX on the fiber cross sections in Fig. 3 are displayed in Table S7 in the supplementary material⁷³ as well. Mapping of Si for the amine-functionalized fiber [Fig. 3(d)] revealed a homogenous distribution over the fiber cross section. Therefore, it is evident that both Al₂O₃ and amine functionalization reach the internal structure of the fiber. From these observations and the results on weight gain saturation (Fig. 1) as well as on chemical states by XPS (Fig. 2), we infer that porous ACF are

functionalized by Al-OH and amine moieties by exposing their internal surface to TMA, H₂O, and azasilane, respectively.

B. Characterization of CO₂ sorption

CO₂ isotherms and pore-size distribution are investigated for the functionalized fiber samples by gas adsorption measurements (Fig. 4). The largest difference in adsorption isotherm is observed for the amine-functionalized sample, when compared to the pristine sample, whereas the Al₂O₃ and Al₂O₃ plus amine-functionalized samples undergo a limited decrease in volume uptake, when compared to the pristine sample [Fig. 4(a)]. The adsorption isotherm for the Al₂O₃ plus amine-functionalized sample deviated slightly from the Al₂O₃-modified fibers. Hysteresis was observed for the amine-functionalized fiber sample, indicating clogging of porosity by amine functionalization. The pore-size distribution [Fig. 4(b)] reveals three distinct pore-size ranges for pristine ACF with diameters of 0.3, 0.5–0.6, and 0.8 nm, respectively. Amine functionalization caused a three- and fourfold decrease in volume associated with the pore-size ranges of 0.5–0.6 and 0.8 nm, respectively, whereas Al₂O₃ modification reduced the volume of the aforementioned pore-size ranges by factor 2. Remarkably, the Al₂O₃ plus amine-functionalized sample revealed the same pore-size distribution as the Al₂O₃-modified sample. As evident from the adsorption isotherms [Fig. 4(a)] and by the lack of change in pore-size distribution [Fig. 4(b)], the exposure of Al₂O₃-modified ACF to azasilane did not clog the porosity, opposite to the case of direct amine functionalization. Instead, functionalization by azasilane is limited on Al₂O₃-modified ACF [Fig. 1(b)]. While the gas exchange was also hampered by Al₂O₃ modification, subsequent functionalization resulted in a >eightfold smaller uptake of azasilane molecules and, hence, did not affect gas exchange as strongly as direct amine functionalization. Further characterization of the full isotherm ($p/p_0 = 1$) was avoided here due to very high CO₂ pressure requirements exceeding the instrumental capacity.

The BET surface area (Table III) derived from argon adsorption isotherms confirms the above-reported conclusions. Amine functionalization reduced the internal surface of the fiber by 50% compared to the pristine fiber, while the internal surface of the Al₂O₃ and Al₂O₃ plus amine functionalization fibers was reduced to 30% of the internal surface of pristine ACF. Also, amine functionalization after Al₂O₃ modification did not decrease the surface area strongly. Evidently, the higher loading of chemisorbed amines (Table III) in direct amine functionalization reduced porosity (Fig. 4) and the BET surface area (Table III). This observation may be rationalized by pore-clogging. In the case of Al₂O₃ plus amine functionalization, Al₂O₃ modification reduces the pore-size *a priori* [Fig. 4(b)], which results in the earlier saturation of amine loading [Fig. 1(b)] and may hamper further and more severe pore-clogging by the subsequent amine functionalization.

To evaluate the influence of different amine loadings and BET surface areas on CO₂ sorption, functionalized and pristine samples were analyzed in the gas exposure setup, where the samples were exposed to dry and humidified synthetic air streams. CO₂ adsorption [Figs. 5(a) and 5(b)] and desorption [Figs. 5(c) and 5(d)] behavior of all samples are investigated by mass spectrometry and the amount of captured CO₂ (Table IV) derived from CO₂

22 September 2023 08:53:50

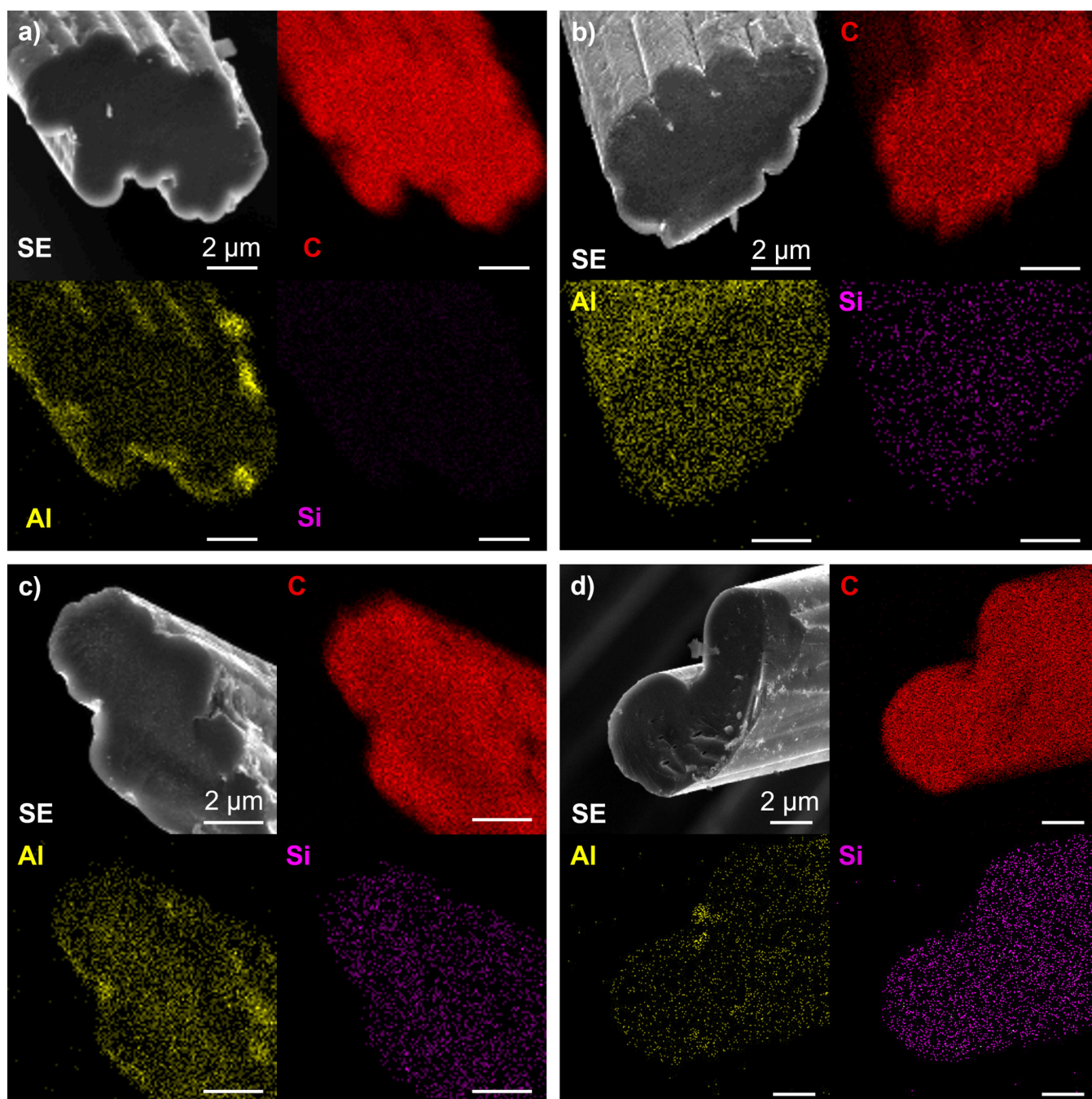


FIG. 3. EDX-mapping of cross sections made from (a) pristine ACF, (b) Al_2O_3 , (c) Al_2O_3 + amine, and (d) amine-functionalized ACF.

concentrations during desorption. During adsorption, the functionalized ACF did not reveal a column-breakthrough behavior, i.e., filtering CO_2 for several minutes from the analyzed stream as observed in previous studies.^{13,21} Instead, only small differences in

CO_2 concentration are detectable during adsorption [Figs. 5(a) and 5(b)] due to the high air permeability of the single layer of the woven ACF cloth utilized in these experiments, which allows air to pass through the cloth without contacting the functionalized fibers.

22 September 2023 08:53:50

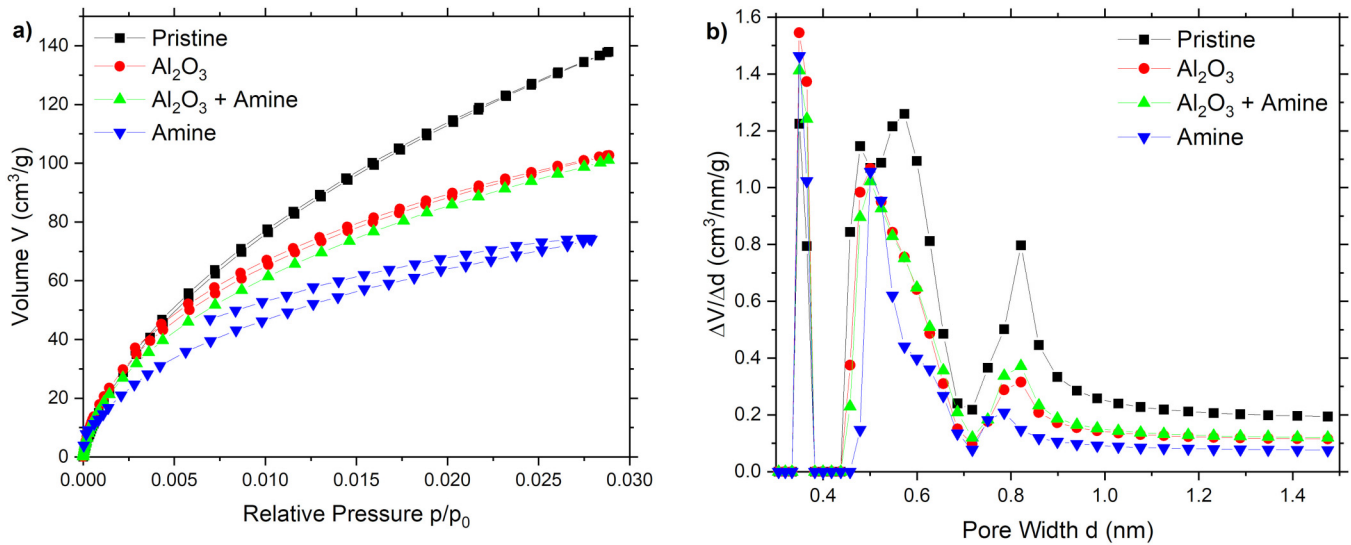


FIG. 4. BET analysis: adsorption isotherms (a) and pore-size distribution (b) of pristine and functionalized ACF.

For desorption, the filter compartment is heated to 80 °C and the desorbed CO₂ is measured in a N₂ purge [Figs. 5(c) and 5(d)]. The delay in the desorption of approximately 700 s was most likely caused by the indirect heating of the sample via an external heater adjacent to the filter compartment. The largest CO₂ desorption was observed for both amine-functionalized samples. Depending on the adsorption conditions, larger quantities of CO₂ desorb from the amine-functionalized samples exposed to humid air, compared [Fig. 5(d)] to dry air [Fig. 5(c)]. The amount of desorbed CO₂ is increased more than twofold for humid adsorption conditions, compared to dry conditions (Table IV). This behavior is ascribed to the additional CO₂-amine reaction in a humid atmosphere resulting in the formation of bicarbonates [Eq. (3) in the supplementary material],⁷³ which is not possible in a dry atmosphere.⁴⁰ As the desorbed CO₂ is removed from the filter compartment in industrial DAC operation and stored or utilized afterward, it is referred to as captured CO₂. However, this figure, while industrially important, does not cover the rate of CO₂ adsorption, as this could not be investigated here due to the air permeability of the ACF cloth during the adsorption experiment [Figs. 5(a) and 5(b)]. Here,

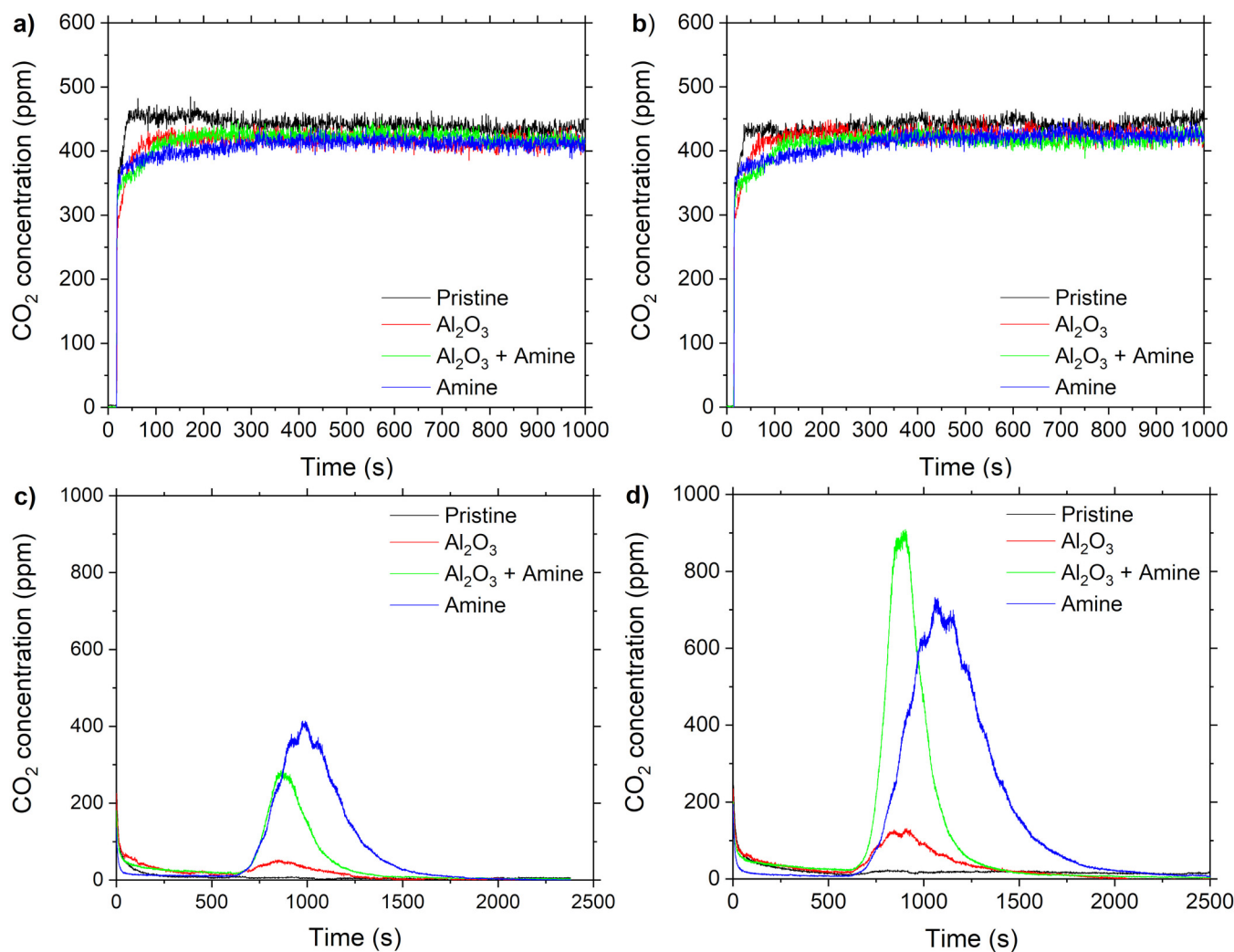
TABLE III. Surface area for pristine and functionalized ACF calculated from BET measurements and loading of amine functionalities derived from the weight gain after functionalization depicted in Fig. 1.

| Functionalization | BET surface area (m ² /g _{sorbent}) | Amine loading (mmol _N /g _{sorbent}) |
|--|---|---|
| Pristine | 1460 ± 150 | ... |
| Al ₂ O ₃ | 1070 ± 110 | ... |
| Al ₂ O ₃ + Amine | 1050 ± 110 | 0.28 ± 0.01 |
| Amine | 760 ± 80 | 2.38 ± 0.01 |

the amounts of CO₂ captured from humid air, 0.18 and 0.13 mmol/g_{sorbent} for the amine and Al₂O₃ plus amine-functionalized samples, respectively, are comparable with DAC by similar sorbents based on functionalized porous silica with reactive amine molecules, which were described at 0.20 mmol/g.^{13,15} Yet, CO₂ capture capacities for polyamine-impregnated systems^{24,29,36} or *in situ* polymerized amines on silica^{25,70,71} were reported in ranges from 0.2 to 2.6 mmol CO₂/g_{sorbent} and, hence, up to more than one order of magnitude higher compared to our work. One reason for this might be the much higher amine loading in these systems, e.g., 7–11 mmol/g_{sorbent} (Ref. 24) or 9.9 mmol/g_{sorbent}²⁵ compared to our work, especially when compared to the amine loading of 0.28 mmol/g_{sorbent} for Al₂O₃ plus amine-functionalized ACF.

While the amount of captured CO₂ is largest for the amine-functionalized sample exposed to humid air compared to the Al₂O₃ plus amine-functionalized carbon cloth, CO₂ desorption from the latter sample occurs within shorter desorption times for the same experimental conditions [Fig. 5(d)]. Therefore, the higher degree of porosity retained by combining Al₂O₃ and amine functionalization (Fig. 4) results in faster CO₂ desorption compared to the solely amine-functionalized sample. Although the amount of captured CO₂ was observed to be 30% less with respect to the amine-functionalized sample, the Al₂O₃ plus amine-functionalized sample revealed a >eightfold reduced amine loading. This implies that amine functionalization on Al₂O₃-modified ACF captured more CO₂ compared to the solely amine-functionalized sample. To calculate the amine efficiency, i.e., the amount of captured CO₂ per amine functionality, two assumptions had to be made for the Al₂O₃ plus amine-functionalized sample. First, the maximum amount of captured CO₂ by Al₂O₃ in this sample did not exceed the 0.039 ± 0.002 mmol/g captured by the solely Al₂O₃-modified sample (Table IV). Second, secondary amine functionalities participated equally in the CO₂-binding reaction as the primary

22 September 2023 08:53:50



22 September 2023 08:53:50

FIG. 5. CO₂ adsorption [(a) and (b)] and desorption [(c) and (d)] monitored by mass spectrometry of pristine and functionalized activated ACF cloth by exposure to dry [(a) and (c)] and humidified [(b) and (d)] synthetic air.

headgroup. These assumptions neglect the chemisorption of azasilane on possible CO₂-binding Al–OH terminations⁷² in the Al₂O₃ plus amine-functionalized sample as well as the potentially reduced CO₂ capturing capacities of secondary amines compared to

primary amines.^{7,15} Altogether, this calculation results in amine efficiencies of 0.31 for CO₂ capture from humid air by the Al₂O₃ plus amine-functionalized sample which exceeds the solely amine-functionalized ACF cloth (Table IV) by a factor of almost 4.

TABLE IV. Amounts of CO₂ desorbed from pristine and functionalized ACF samples calculated from the desorption experiments shown in Fig. 5.

| Functionalization | Amount of captured CO ₂ from | | Amine efficiency for | |
|--|---|--|----------------------|---------------|
| | Dry air (mmol/g _{sorbent}) | Humid air (mmol/g _{sorbent}) | Dry air (–) | Humid air (–) |
| Pristine | 0.010 ± 0.002 | 0.033 ± 0.002 | ... | ... |
| Al ₂ O ₃ | 0.021 ± 0.002 | 0.039 ± 0.002 | ... | ... |
| Al ₂ O ₃ + Amine | 0.049 ± 0.001 | 0.127 ± 0.001 | 0.10 | 0.31 |
| Amine | 0.083 ± 0.001 | 0.183 ± 0.001 | 0.04 | 0.08 |

Efficiencies for CO₂ capture from dry air are reduced in the same way as the amount of captured CO₂ compared to humid air experiments. Still, they reveal a larger efficiency for the Al₂O₃ plus amine-functionalized sample compared to the solely amine-functionalized sample. However, contributions to CO₂ capture (Fig. 5) are not restricted to amine functionalization, but also physisorption and, in case of the humid atmosphere, CO₂ dissolution in pore-confined H₂O might have occurred, although amine-free samples, pristine and Al₂O₃-modified ACF revealed little CO₂ capture (Table IV). Therefore, efficiencies of amine-functionalized ACF require further investigations beyond the scope of this work.

Yet, the efficiency figure of 0.31 for the Al₂O₃ plus amine-functionalized sample highlights the great potential of ACF-based sorbents, where the combination of Al₂O₃ modification preceding amine functionalization prevents the twofold porosity reduction observed for the solely amine-functionalized surface (Table III). In fact, comparable systems of chemisorbed amines on porous silica^{7,13,15,21} reveal amine efficiencies between 0.07 and 0.2, while their functionalization reduces the surface area of porous supports by approximately 50%^{13,15} (Table I) to 216 and 230 m²/g. Direct amine functionalization for these systems as well as for the ACF cloth resulted in high amine loading but reduced contribution in CO₂-binding reactions. Moreover, our experiments reveal that the regeneration time of the sorbent material takes 1200 s as CO₂ desorption is hampered in the amine-functionalized sample (Fig. 5). On the contrary, the fast and steady CO₂ desorption observed for the Al₂O₃ plus amine-functionalized sample indicated little hindrance for CO₂ release from the internal surface. Also, all other amine-based DAC sorbents reported in Table I did not exceed amine efficiencies of 0.22,²³ while adsorption and desorption cycles were performed for several hours compared to 6 min long cycles applied in this work. In conclusion, we infer that the combination of ALD Al₂O₃-modified and amine-functionalized ACF is compatible with DAC applications. Yet, more research is necessary to determine the cycle life, sorption mechanisms, and the degradation of amine-functionalized ACF, especially in humid environments.

IV. SUMMARY AND CONCLUSIONS

ACF cloths were functionalized with CO₂ adsorbing amine moieties by using vapor-phase surface functionalization. XPS analysis confirmed the chemical modification by Al₂O₃ and amine functionalities anchored via –Si–O–C/–Si–O–Al bridges. Fiber cross sections investigated by SEM and EDX-mapping revealed a homogeneous distribution of Al and Si indicating the functionalization of the complete internal surface together with the weight gain saturation after functionalization, compared to the pristine samples. Yet, functionalization changed the internal surface and its pore-size distribution as evident from gas adsorption measurements. While Al₂O₃ modification and the combination of Al₂O₃ and subsequent amine functionalization reduced the internal surface by 30%, amine functionalization on pristine ACF reduced the internal surface to 50% of the pristine substrate. The amine-functionalized sample revealed the highest amount of adsorbed CO₂ (0.18 mmol/g_{sorbent}) caused by high amine loading but at the cost of a long overall CO₂ desorption time. Instead, the retained porosity on

Al₂O₃ processing and, subsequently, amine-functionalizing allowed for fast gas exchange and CO₂ capture capacities of 0.13 mmol/g_{sorbent}, although the overall amine loading is at least a factor 8 smaller than in the case of direct amine-functionalized ACF (Table III). Thus, the capturing or amine efficiency for the combination of Al₂O₃ plus amine functionalization reached 0.31 mol CO₂ per mol of amine functionalities superior to direct amine functionalization. Our findings demonstrate that for direct air capture, not only the overall loading of CO₂ adsorbing species, but their effect on the internal surface of the porous support must be considered and engineered for future efficient sorption of CO₂ from the ambient air. ACF supports represent an important alternative to the widely used porous silica for DAC application due to their high thermal conductivity and high degree of porosity. By preserving this porosity by tailored functionalization, here, ALD Al₂O₃ and subsequent amine functionalization resulted in superior efficiency figures for CO₂ capture. Future studies will focus on increasing amine loading, optimizing sorbent porosity, the interaction between Al₂O₃ and amine functionalization, long-term stability experiments, and process development to efficiently meet demands for large area functionalization, e.g., in pilot plants. Increased amine loadings and specially designed or engineered ACF supports, e.g., by ALD, together might pave the way toward realizing efficient DAC.

ACKNOWLEDGMENTS

The authors acknowledge financial support via the Eindhoven Engine Project “Carbyon DAC” (No. 2020-101). S.P. and G.v.S. are grateful for the technical support and discussions with Cristian van Helvoirt, Caspar van Bommel, Joris Meulendijks, and Janneke Zeebregts at TU/e.

AUTHOR DECLARATIONS

Conflict of Interest

D.v.E. and H.d.N. have a financial interest in Carbyon Holding BV. The authors do not believe this had any influence on the results published in this paper.

Author Contributions

Stephan Prünte: Conceptualization (equal); Data curation (equal); Formal analysis (equal); Investigation (equal); Methodology (equal); Validation (equal); Writing – original draft (equal); Writing – review & editing (equal). **Gerben van Straaten:** Conceptualization (equal); Formal analysis (equal); Investigation (equal); Methodology (equal); Writing – review & editing (equal). **Dries van Eyck:** Formal analysis (equal); Investigation (equal); Methodology (equal); Writing – review & editing (equal). **Oscar Diaz-Morales:** Formal analysis (supporting); Investigation (equal); Methodology (supporting); Writing – review & editing (equal). **Jeroen Van Dijck:** Formal analysis (equal); Investigation (equal); Methodology (equal); Writing – review & editing (equal). **Hans de Neve:** Conceptualization (equal); Formal analysis (supporting); Funding acquisition (equal); Investigation (supporting); Methodology (supporting); Project administration (equal); Resources (equal); Writing – review & editing (equal).

Mariadriana Creatore: Conceptualization (equal); Formal analysis (equal); Funding acquisition (equal); Investigation (equal); Methodology (equal); Project administration (equal); Resources (equal); Supervision (equal); Writing – review & editing (equal).

DATA AVAILABILITY

The data that support the findings of this study are available from the corresponding author upon reasonable request.

REFERENCES

- ¹J. Meckling and E. Biber, *Nat. Commun.* **12**, 2051 (2021).
- ²J. C. Minx *et al.*, *Environ. Res. Lett.* **13**, 063001 (2018).
- ³S. Fuss *et al.*, *Environ. Res. Lett.* **13**, 063002 (2018).
- ⁴D. P. van Vuuren *et al.*, *Nat. Clim. Change* **8**, 391 (2018).
- ⁵P. R. Shukla, J. Skea, R. Slade, and A. Al Khourdajie, “Climate change 2022: Mitigation of climate change,” in *Contribution of Working Group III to the Sixth Assessment Report of the Intergovernmental Panel on Climate Change*, edited by P. R. Shukla, J. Skea, R. Slade, and A. Al Khourdajie (Cambridge University, Cambridge, 2022).
- ⁶N. McQueen, K. V. Gomes, C. McCormick, K. Blumanthal, M. Pisciotto, and J. Wilcox, *Prog. Energy* **3**, 032001 (2021).
- ⁷E. S. Sanz-Pérez, C. R. Murdock, S. A. Didas, and C. W. Jones, *Chem. Rev.* **116**, 11840 (2016).
- ⁸D. W. Keith, G. Holmes, D. St. Angelo, and K. Heidel, *Joule* **2**, 1573 (2018).
- ⁹X. Shi, H. Xiao, H. Azarabadi, J. Song, X. Wu, X. Chen, and K. S. Lackner, *Angew. Chem. Int. Ed.* **59**, 6984 (2020).
- ¹⁰C. Hepburn, E. Adlen, J. Beddington, E. A. Carter, S. Fuss, N. Mac Dowell, J. C. Minx, P. Smith, and C. K. Williams, *Nature* **575**, 87 (2019).
- ¹¹C. Beuttl, L. Charles, and J. Wurzbacher, *Front. Clim.* **1**, 10 (2019).
- ¹²S. Deutz and A. Bardow, *Nat. Energy* **6**, 203 (2021).
- ¹³J. A. Wurzbacher, C. Gebald, and A. Steinfeld, *Energy Environ. Sci.* **4**, 3584 (2011).
- ¹⁴M. Fasihi, O. Efimova, and C. Breyer, *J. Clean. Prod.* **224**, 957 (2019).
- ¹⁵S. A. Didas, A. R. Kulkarni, D. S. Sholl, and C. W. Jones, *ChemSusChem* **5**, 2058 (2012).
- ¹⁶C. M. Liu, N. K. Sandhu, S. T. McCoy, and J. A. Bergerson, *Sustain. Energy Fuels* **4**, 3129 (2020).
- ¹⁷M. M. de Jonge, J. Daemen, J. M. Loriaux, Z. J. Steinmann, and M. A. Huijbregts, *Int. J. Greenh. Gas Con.* **80**, 25 (2019).
- ¹⁸M. Jahandar Lashaki and A. Sayari, *Chem. Eng. J.* **334**, 1260 (2018).
- ¹⁹A. Heydari-Gorji, Y. Yang, and A. Sayari, *Energy Fuels* **25**, 4206 (2011).
- ²⁰H. T. Kwon, M. A. Sakwa-Novak, S. H. Pang, A. R. Sujana, E. W. Ping, and C. W. Jones, *Chem. Mater.* **31**, 5229 (2019).
- ²¹Y. Belmabkhout, R. Serna-Guerrero, and A. Sayari, *Chem. Eng. Sci.* **65**, 3695 (2010).
- ²²P. J. E. Harlick and A. Sayari, *Ind. Eng. Chem. Res.* **46**, 446 (2007).
- ²³S. H. Pang, L.-C. Lee, M. A. Sakwa-Novak, R. P. Lively, and C. W. Jones, *J. Am. Chem. Soc.* **139**, 3627 (2017).
- ²⁴D. R. Kumar, C. Rosu, A. R. Sujana, M. A. Sakwa-Novak, E. W. Ping, and C. W. Jones, *ACS Sustainable Chem. Eng.* **8**, 10971 (2020).
- ²⁵S. Choi, J. H. Drese, P. M. Eisenberger, and C. W. Jones, *Environ. Sci. Technol.* **45**, 2420 (2011).
- ²⁶W. Chaikittisilp, H.-J. Kim, and C. W. Jones, *Energy Fuels* **25**, 5528 (2011).
- ²⁷Y. Liu, B. Sajjadi, W.-Y. Chen, and R. Chatterjee, *Fuel* **247**, 10 (2019).
- ²⁸S. Choi, T. Watanabe, T.-H. Bae, D. S. Sholl, and C. W. Jones, *J. Phys. Chem. Lett.* **3**, 1136 (2012).
- ²⁹A. R. Sujana, S. H. Pang, G. Zhu, C. W. Jones, and R. P. Lively, *ACS Sustainable Chem. Eng.* **7**, 5264 (2019).
- ³⁰D. Saha and H. A. Grappe, in *Activated Carbon Fiber and Textiles*, edited by J. Y. Chen (Woodhead Publishing, Duxford, 2017), p. 143.
- ³¹J. A. Mason, T. M. McDonald, T.-H. Bae, J. E. Bachman, K. Sumida, J. J. Dutton, S. S. Kaye, and J. R. Long, *J. Am. Chem. Soc.* **137**, 4787 (2015).
- ³²R. Rodríguez-Mosqueda, E. A. Bramer, T. Roestenberg, and G. Brem, *Ind. Eng. Chem. Res.* **57**, 3628 (2018).
- ³³N. N. Meis, A. M. Frey, J. H. Bitter, and K. P. de Jong, *Ind. Eng. Chem. Res.* **52**, 12812 (2013).
- ³⁴N. Masoud, G. Bordanaba-Florit, T. van Haasterecht, and J. H. Bitter, *Ind. Eng. Chem. Res.* **60**, 13749 (2021).
- ³⁵Z. Hu, Y. Wang, B. B. Shah, and D. Zhao, *Adv. Sustainable Syst.* **3**, 1800080 (2019).
- ³⁶W. C. Wilfong, Q. Wang, T. Ji, J. S. Baker, F. Shi, S. Yi, and M. L. Gray, *Energy Technol.* **10**, 2200356 (2022).
- ³⁷S. L. Di Vittorio, M. S. Dresselhaus, M. Endo, J.-P. Issi, L. Piroux, and V. Bayot, *J. Mater. Res.* **6**, 778 (1991).
- ³⁸Y. Belmoujahid, M. Bonne, Y. Scudeller, D. Schleich, Y. Grohens, and B. Lebeau, *Eur. Phys. J. Spec. Top.* **224**, 1775 (2015).
- ³⁹Y. Belmoujahid, M. Bonne, Y. Scudeller, D. Schleich, Y. Grohens, and B. Lebeau, *Microporous Mesoporous Mater.* **201**, 124 (2015).
- ⁴⁰A. E. Szego, A. Jaworski, and N. Hedin, *Mater. Adv.* **2**, 448 (2021).
- ⁴¹J. Yu and S. S. C. Chuang, *Energy Fuels* **30**, 7579 (2016).
- ⁴²R. Afonso, M. Sardo, L. Mafra, and J. R. B. Gomes, *Environ. Sci. Technol.* **53**, 2758 (2019).
- ⁴³B. Aziz, N. Hedin, and Z. Bacsik, *Microporous Mesoporous Mater.* **159**, 42 (2012).
- ⁴⁴S. A. Didas, M. A. Sakwa-Novak, G. S. Foo, C. Sievers, and C. W. Jones, *J. Phys. Chem. Lett.* **5**, 4194 (2014).
- ⁴⁵T. C. Drage, A. Arenillas, K. M. Smith, and C. E. Snape, *Microporous Mesoporous Mater.* **116**, 504 (2008).
- ⁴⁶B. Arkles, Y. Pan, G. L. Larson, and D. H. Berry, in *Silanes and Other Coupling Agents*, edited by K. L. Mittal (CRC, Hoboken, 2004), Vol. 3, p.179.
- ⁴⁷L. Ju and N. C. Strandwitz, *J. Mater. Chem. C* **4**, 4034 (2016).
- ⁴⁸B. Arkles, J. Goff, T. Min, Y. Pan, A. Phillips, K. DeMella, and C. Brick, *ACS Appl. Mater. Interfaces* **12**, 27737 (2020).
- ⁴⁹R. Walsh, *Acc. Chem. Res.* **14**, 246 (1981).
- ⁵⁰A. F. Maddox, J. G. Matison, M. Singh, J. Zazyczny, and B. Arkles, *MRS Proc.* **1793**, 35 (2015).
- ⁵¹S. B. S. Heil, E. Langereis, F. Roozeboom, M. C. M. van de Sanden, and W. M. M. Kessels, *J. Electrochem. Soc.* **153**, G956 (2006).
- ⁵²J. Jagiello and M. Thommes, *Carbon* **42**, 1227 (2004).
- ⁵³Z. Yue and J. Economy, in *Activated Carbon Fiber and Textiles*, edited by J. Y. Chen (Woodhead Publishing, Duxford, 2017), p. 61.
- ⁵⁴M. Suzuki, *Carbon* **32**, 577 (1994).
- ⁵⁵P. M. Dietrich, N. Graf, T. Gross, A. Lippitz, S. Krakert, B. Schüpbach, A. Terfort, and W. E. S. Unger, *Surf. Interface Anal.* **42**, 1184 (2010).
- ⁵⁶K. Artyushkova, *J. Vac. Sci. Technol. A* **38**, 031002 (2020).
- ⁵⁷I. M. El Nahhal, M. M. Chehimi, C. Cordier, and G. Dodin, *J. Non-Cryst. Solids* **275**, 142 (2000).
- ⁵⁸I. Matanovic, K. Artyushkova, and P. Atanassov, *Curr. Opin. Electrochem.* **9**, 137 (2018).
- ⁵⁹N. Hellgren, R. T. Haasch, S. Schmidt, L. Hultman, and I. Petrov, *Carbon* **108**, 242 (2016).
- ⁶⁰Y. L. Khung, S. H. Ngalim, A. Scaccabarozzi, and D. Narducci, *Beilstein J. Nanotechnol.* **6**, 19 (2015).
- ⁶¹Y.-S. Wang *et al.*, *Electrochim. Acta* **87**, 261 (2013).
- ⁶²S.-Y. Yang, K.-H. Chang, H.-W. Tien, Y.-F. Lee, S.-M. Li, Y.-S. Wang, J.-Y. Wang, C.-C. M. Ma, and C.-C. Hu, *J. Mater. Chem.* **21**, 2374 (2011).
- ⁶³A. Avila, I. Montero, L. Galán, J. M. Ripalda, and R. Levy, *J. Appl. Phys.* **89**, 212 (2001).
- ⁶⁴J. Chastain, *Handbook of X-ray Photoelectron Spectroscopy* (Perkin-Elmer Corporation, Eden Prairie, MN, 1992).
- ⁶⁵L. Ju, B. Bao, S. W. King, and N. C. Strandwitz, *J. Vac. Sci. Technol. A* **35**, 01B136 (2017).
- ⁶⁶S. Ben Amor, G. Baud, M. Jacquet, G. Nansé, P. Fioux, and M. Nardin, *Appl. Surf. Sci.* **153**, 172 (2000).

⁶⁷I. Olefjord, H. J. Mathieu, and P. Marcus, *Surf. Interface Anal.* **15**, 681 (1990).

⁶⁸G. Dingemans and W. M. M. Kessels, *J. Vac. Sci. Technol. A* **30**, 040802 (2012).

⁶⁹E. Hoque, J. A. DeRose, P. Hoffmann, B. Bhushan, and H. J. Mathieu, *J. Phys. Chem. C* **111**, 3956 (2007).

⁷⁰K. A. S. Abhilash, T. Deepthi, R. A. Sadhana, and K. G. Benny, *ACS Appl. Mater. Interfaces* **7**, 17969 (2015).

⁷¹F.-Q. Liu, L. Wang, Z.-G. Huang, C.-Q. Li, W. Li, R.-X. Li, and W.-H. Li, *ACS Appl. Mater. Interfaces* **6**, 4371 (2014).

⁷²M. E. Potter, K. M. Cho, J. J. Lee, and C. W. Jones, *ChemSusChem* **10**, 2192 (2017).

⁷³See the supplementary material at <https://www.scitation.org/doi/suppl/10.1116/6.0002419> for additional information on CO₂ capture with amines and further details on the XPS peak fitting procedures and SEM/EDX analysis employed in this work.